Ab initio study of the structural, electronic, and magnetic properties of MnO(100) and MnO(110)

V. Bayer,* C. Franchini,† and R. Podloucky
Department of Physical Chemistry, University of Vienna, Sensengasse 8, A-1090, Vienna, Austria
(Received 20 September 2006; revised manuscript received 9 November 2006; published 2 January 2007)

The structural, electronic, and magnetic properties of the MnO(100) and (110) surfaces were studied within the standard approximation of Perdew, Burke, and Ernzerhof (PBE) and the PBE+U approach. For the (100) surface, the surface layers relax inwards for both sets of calculations. For the (110) surface an electronically driven missing row reconstruction is predicted which significantly lowers the surface energy. For all cases, the O surface atoms relax outwards in comparison to Mn, inducing a buckling of the surface layers. The antiferromagnetic type II ordering of the bulk phase is conserved for both surfaces, the local magnetic moments of Mn exhibit no change with respect to the bulk values. The magnetic ordering at the surfaces is studied in terms of the Heisenberg model and the calculated exchange coupling constants as derived from the *ab initio* data are significantly enhanced at the surface with respect to the bulk.

DOI: 10.1103/PhysRevB.75.035404 PACS number(s): 68.47.Gh, 68.35.Bs, 71.27.+a, 75.30.Et

I. INTRODUCTION

Mn monoxide is long known as a material whose specific electronic and magnetic structure constitutes a challenge for *ab initio* calculations due to the half-filled *d*-states of Mn. It is well-known that, despite its remarkable successes in describing the properties of condensed matter, density functional theory (DFT) within the standard local density approximation (LDA) and generalized gradient approximation (GGA) turns out to be inadequate in describing the physics of systems with strongly localized electrons. This limitation arises from the wrong treatment of the self-interaction energy which is wrongly included in the basic LDA and GGA formalism.[1] As a consequence, fundamental quantities such as the magnitude of the magnetic moment or the value of the gap in insulating materials, are seriously underestimated,[2] thus affecting the reliability of the results. A variety of studies on bulk MnO exist, which particularly deal with aspects of exchange and correlation of the localized *d*-states. An overview concerning calculations for bulk MnO can be found in one of our recent papers.[3] Recently, also the polar (111) surface was investigated.[4] For this orientation surface reconstructions have been characterized as a function of O partial pressure. In the present paper, we will focus on the (100) and (110) surfaces of MnO, discussing their structural, electronic, and magnetic properties.

The number of studies on the properties of manganese oxide surfaces is very limited. For the (100) surface a few studies were performed, experimentally[5–10] as well as theoretically.[10,11] Thin layers of 5 to 7 monolayers of MnO(100) can be grown on Ag(100) at low temperatures[8] and in a narrow range of the O partial pressure of 10^{-8} to 5×10^{-7} mbar. Upon other temperature and pressure conditions the more O-rich Mn_3O_4 and Mn_2O_3 phases are formed. Data of low energy electron diffraction (LEED)[6] studies for MnO(100) at elevated temperatures indicate that 2×2 and 6×6 reconstructions occur, which are stable in temperature ranges of 800–480 K and 1000–298 K, respectively. For both types of reconstructions, a small buckling of the surface plane was derived, which agrees with the more recent LEED results of Soares *et al.*[9] However, based on a medium energy ion scattering (MEIS) experiment by Okazawa,[10] opposite buckling effects were claimed. Also the two theoretical studies of Refs. 10 and 11 resulted in contradicting values.

Magnetic and electronic properties of late transition metal oxides are particularly intriguing. In general, pronounced surface induced features may occur, such as changes of the coordination of the metal atoms, complex reconstructions, and modifications of the spin and charge density distribution. These surface effects might strongly influence the magnetic structure by inducing magnetic moments on O atoms at the surface, changing the super-exchange interactions,[12] reducing the magnetic moment of the metal atom, and forming incommensurable magnetic structures.[13] On the other hand, strong changes are not expected for insulators. The LDA based DFT study of Momida and Oguchi[11] for MnO(100) reports that surface and subsurface O atoms gain a finite (but rather small) magnetic moment and furthermore the insulating character of bulk MnO is preserved at the surface because the band gap is reduced only by a small amount.

The surface structure of MnO(100) is still under debate: the main conflicting points concern the relaxation of the surface layers and their buckling, namely whether the O atoms (LEED,[6,9] and MD[10]) or the Mn atoms (MEIS[10] and DFT-LDA[11]) relax outwards. In this work, we present an extensive study of the clean MnO(100) and (110) surfaces by means of the PBE+U method, in order to derive structural magnetic and electronic properties with one of the most precise methods. To underline the achievements of the PBE+U approach, a detailed comparison to standard PBE calculations will be made. We focus our attention on surface energies, surface reconstructions, the electronic structure, and the magnetic ordering in terms of the Heisenberg model deriving exchange coupling parameters.

II. COMPUTATIONAL ASPECTS

A. Methodology

Density functional theory calculations were performed by means of the *Vienna Ab initio Simulation Package* (VASP)[14,15] within the projector augmented wave construction for the

TABLE I. Bulk interlayer distances d_{bulk} (in Å) for MnO(100) and (110).

	exp	PBE	PBE+U
(100)	2.215,[23] 2.222[24]	2.216	2.248
(110)	1.566,[23] 1.571[24]	1.545	1.585

core potentials.[16,17] Exchange and correlation were treated within the generalized gradient approximation of Perdew *et al.* (PBE).[18] Calculations in the spirit of the Hubbard model[19] using Dudarev's approach[20] were performed by fixing the value $U-J$ to 6 eV, which is the optimized choice for bulk MnO.[3] The energy cutoff of the plane wave basis was 350 eV. The surfaces were modeled by repeated slabs with symmetric terminations with a vacuum spacing of about 15 Å, applying the theoretically optimized bulk lattice parameters[3] of a_{PBE}=4.369 Å, and a_{PBE+U}=4.479 Å, for the PBE and PBE+U calculations, accordingly. The convergency of total energies was tested with respect to the number of layers and the $\bar{k}$ mesh. For the (100) surface nine layers turned out to be sufficient whereas for the (110) surface at least 11 layers need to be chosen. The Brillouin zone integration was done by the technique of Methfessel and Paxton[21] with a smearing of half width of 0.2 eV. The grid of $\bar{k}$ points was generated according to Monkhorst and Pack.[22] A Γ-centered grid of $5\times5\times1$ for both surfaces was applied. Because of the antiferromagnetic type-II ordering, the smallest two-dimensional cells for both surfaces are of $p(2\times1)$ type. For the investigation of the missing row (MR) reconstruction of the (110) surface a $p(2\times2)$ supercell was constructed retaining the $\bar{k}$ mesh. An overview of the bulk interlayer distances for both orientations can be found in Table I. Relaxations of all atomic positions were allowed by minimizing the atomic forces but fixing the positions of atoms in the central layer.

Below the Néel temperature of T_N=118 K, MnO crystallizes in a rhombohedrally distorted B1 structure[3] with a distortion angle smaller than 1°. This distortion changes the cubic lattice to a rhombohedral lattice because of a uniaxial compression along the [111] direction. Consequently, for the calculation of the (100) surface a trigonal setup was chosen. In the case of the computationally more demanding calculation of the (110) surface and its MR reconstruction a simple tetragonal cell was chosen but the atoms were allowed to follow the experienced small lateral forces.

B. Surface energy

The surface energy γ derived for a symmetric slab is given by

$$\gamma=(E^{slab}-nE^{bulk}_{\mathrm{MnO}})/(2A)$$

in which the energy E^{slab} is the total energy of the slab, and E^{bulk}_{MnO} is the bulk total energy. n denotes the number of MnO formula units, and A is the area of the two-dimensional unit cell. The values of the bulk total energies per formula unit are −16.67 and −15.24 eV for the PBE and PBE+U calculations, respectively. The factor 2 takes into account that the slabs are terminated by two equivalent surfaces.

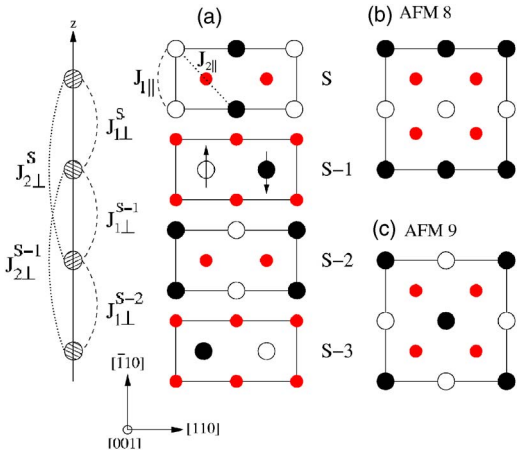

FIG. 1. (Color online) (a) illustrates the geometric and magnetic AFM II structure of four sequential layers of MnO(100). S denotes the surface layer, S-1 the subsurface layer, and so on. Black and white circles indicate Mn magnetic moments up and down, respectively; grey (red) circles refer to O atoms. The magnetic ordering for the AFM 8 and AFM 9 arrangements is shown in (b) and (c), respectively. An illustrated picture of the nearest (J_1) and second nearest (J_2) coupling constants is given on the left. $J_\perp$ denotes interlayer coupling constants, whereas $J_\parallel$ denotes intralayer coupling constants.

C. Exchange coupling constants

The magnetic ordering of bulk MnO is antiferromagnetic (AFM type II), i.e., magnetic moments are aligned parallel within the (111) planes and antiparallel between adjacent planes. Figures 1(a) and 2(a) show the first four surface lay-

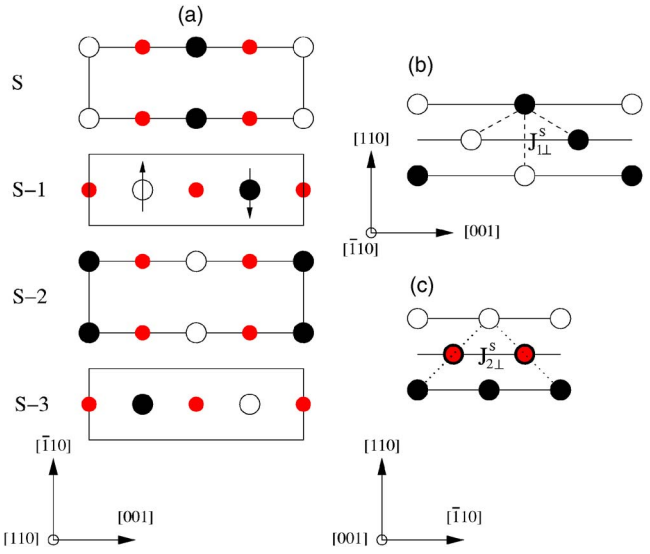

FIG. 2. (Color online) (a) Geometric and magnetic AFM II structure of four sequential layers of MnO(110). (b) and (c): Side views with an illustration of nearest (J_1) and second nearest neighbor (J_2) exchange coupling constants, respectively.

TABLE II. ΔE gives the total energy differences (per 1×1 unit cell) relative to an AFM II ordered slab. The magnetic configuration is sketched with + and − labels, indicating spin ↑ and ↓, respectively. The symbol ± denotes a mixed spin configuration within the surface layer.

	(100)		(110)		(110) MR	
Magnetic ordering	Spin configuration	ΔE (meV)	Spin configuration	ΔE (meV)	Spin configuration	ΔE (meV)
AFM II		0		0		0
FM	+++++++	264	+++++++++	313	++++++++++	375
AFM 1	+++−+++	178	++++−++++	199	+++++−+++++	262
AFM 2	++−+−++	103	+++−+−+++	166	++−++++−++	150
AFM 3	+−++++−	94	−+−++++−+−	41	−−+−++++−+−−	68
AFM 4	−++++−	157	−++++++−	162	−+++++++++−	290
AFM 5	−−+++−−	157	−−++++−−	163	−−++++++−−	205
AFM 6	+−+−+−+	37	+−+−+−+−+	15	+−+−+−+−+−+	31
AFM 7	−++−++−	72	++−+−+−++	44	++−+−+−+−++	38
AFM 8	±++++±±	191			−−−++++−−−	215
AFM 9	∓++++∓∓	171			+−−−+++−−−+	132

ers of the (100) and (110) terminations, correspondingly; at and below the fifth layer the magnetic ordering reiterates.

To investigate the effect of the surface on the magnetic structure and to evaluate its stability, exchange coupling constants were calculated within the PBE+U approach applying a tetragonal unit cell. Standard GGA and LDA approaches were not considered since they fail to describe the coupling constants in highly correlated materials, providing usually much too large values.[3,25] Table II lists the different magnetic configurations and the relative stabilities of the different orderings used to evaluate the exchange coupling constants. If not noted otherwise a 1×1 two-dimensional surface unit cell was applied. Therefore all spins within one layer are coupled ferromagnetically. The slabs consist of 7, 9, and 11 layers for the (100), (110), and (110) MR surface, respectively. To obtain $J_{\parallel}$ for the (100) surface, two additional magnetic orderings, AFM 8 and AFM 9 (see Fig. 1), in a $p(2\times1)$ and a $p(2\times2)$ cell, respectively, were considered. We used a Heisenberg model for localized magnetic moments following the ansatz of Ködderitzsch *et al.*,[26] who applied it to the study of NiO(100). The layer dependent Heisenberg Hamiltonian H for magnetic interaction between nearest neighbors (NN) and next nearest neighbors (NNN) is given by

$$H=\sum_{NN} J_1\mathbf{S_i}\mathbf{S_j}+\sum_{NNN} J_2\mathbf{S_i}\mathbf{S_j} \qquad (1)$$

Based on PBE+U total energies corresponding to different magnetic orderings within the slab, the exchange coupling constants can be derived from a proper set of equations involving total energy differences (see the Appendix). A recent review on the theoretical description of magnetic interactions can be found in Ref. 27. We consider only nearest neighbor (J_1) and next nearest neighbor (J_2) interactions. Higher order terms can be safely neglected, as argued, e.g., by Lines[28,29] and Oguchi *et al.*[30] Surface dependency of the constants J_1 and J_2 is introduced by splitting the exchange energy into interlayer ($J_{\perp}$) and intralayer ($J_{\parallel}$) interactions. A schematic representation of the exchange interactions is given by Figs. 1 and 2. For the MnO(100), $J_{\perp}$ couples spins placed on adjacent planes. For the (110) orientation each magnetic moment in the surface plane S couples to four nearest neighbor moments in the subsurface layer S-1 and to one nearest moment in plane S-2. Similar to our bulk study[3] any canting of the spins (i.e., $\mathbf{S_i}\mathbf{S_j}=S^2$) is neglected for the actual derivation of the coupling constants and we set $S=5/2$, corresponding to an Mn^{2+} ion with five half-filled d-states. Only magnetic configurations which are symmetric with respect to the central plane of the slab have been considered. A more detailed description of the magnetic arrangements will be given later on. Since the exchange coupling parameters were derived from geometrically relaxed calculations they have to be viewed as a kind of effective surface exchange coupling constants.

III. RESULTS AND DISCUSSION

A. Energetics

Table III summarizes the calculated surface energies. The values show that both methods, PBE and PBE+U, favor the (100) surface, in agreement with experiment. The PBE+U surface energy of $\gamma=54$ meV/Å^2 is in good agreement with the result of Momida and Oguchi[11] (56 meV/Å^2), which was

TABLE III. Calculated surface energy γ for the (100), (110), and the (110) MR surfaces of MnO. Both PBE and PBE+U results are listed in the table.

	PBE		PBE+U	
γ	eV/Å^2	J/m^2	eV/Å^2	J/m^2
(100)	0.045	0.71	0.054	0.86
(110)	0.082	1.31	0.108	1.73
(110) MR	0.058	0.93	0.078	1.25

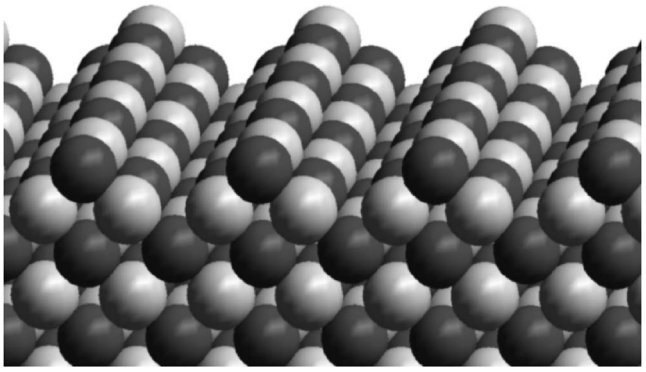

FIG. 3. A perspective view of the (110) MR surface, which is obtained by removal of half of the surface atoms.

derived by applying a full-potential linearized plane wave method within the LDA functional (DFT-LDA). When the (110) surface undergoes the missing row reconstruction, obtained by removing every second surface O-Mn-O row aligned along the [100] direction (see Fig. 3), its surface energy is significantly lowered by ≈30%.

It is also noticeable that the relative stabilities, i.e., differences of surface energies for PBE and PBE+U, are rather comparable (although slightly enhanced for the PBE+U calculation).

Our findings remind us of those observed in NiO.[26,28,29,31–37] Indeed, due to its similar structural, electronic, and magnetic properties NiO is often taken as a touchstone for MnO. In NiO (Ref. 31) the (100) termination is by 0.15 eV/Å^2 (2.4 J/m^2) more stable than the unreconstructed (110) surface. Reconstruction effects are reported for the (110) termination,[32,33] consisting of (100) and (010) facets, whose size vary upon temperature up to several nanometers. We should remark that due to the lack of experimental results guiding our theoretical investigation, we restrict our study to the basic MR reconstruction, therefore the formation of more complex reconstructions cannot be excluded *a priori*. As we will show later on, the driving force for the MR reconstruction is the stabilization of the insulating character and the magnetic ordering which would be otherwise lost for an unreconstructed surface.

B. Structural properties

Compared to the flat MnO(100), the (110) surface is more open since the subsurface layer atoms are not directly situated beneath the topmost atoms (see Fig. 2), therefore relaxation effects are expected to be larger. The compilation of the optimized geometry for both surfaces is listed in Table IV along with available experimental measurements and previous theoretical estimations.

As anticipated in the Introduction, the structural properties of the clean (100) surface are a controversial topic. In analogy to other divalent metal oxides, Prutton *et al.*[38] indicated that MnO(100) has a structure close to a simple termination of the bulk lattice and suggested a buckling of the surface of ±3%, probably resulting from an outward displacement of surface O and a smaller inward contraction of the topmost Mn atoms.[6] However, due to acute difficulties in treating transition metal oxides, the authors were unable to obtain a physically reasonable picture of the ionic relax-

TABLE IV. Calculated optimized geometry for the MnO(100), MnO(110), and MnO(110) MR surfaces in terms of interlayer relaxation (d_{ij}) and buckling (b_i), both given in percent with respect to the bulk interlayer distance. A positive value of b_i indicates an outward relaxation of O relative to Mn, whereas a negative value an inward relaxation, correspondingly. When available, other theoretical estimations along with experimental data are also included.

	d_{12}	d_{23}	d_{34}	d_{45}	b_1	b_2	b_3
			MnO (100)				
			Theory				
DFT-LDA[11]	−1.5	−0.1	0.2		−0.5	−1.4	0.0
MD[10]	−2.9	1.6			1.7	−1.6	
			Experiment				
MEIS[10]	0.1±0.7	−1.0±0.7			−3.6±0.7	−2.0±0.7	
LEED[9]	1.1±2.5				5.5±2.5	0.5±2.5	
			This work				
PBE	−1.6	0.3	0.2	0.4	1.6	−1.6	0.3
PBE+U	−0.3	0.4	0.5	0.6	1.3	−0.4	0.0
			MnO (110)				
PBE	−8.6	5.9	1.2	3.1	3.4	−9.4	2.4
PBE+U	−8.6	5.1	−1.0	1.3	2.7	−2.6	0.6
			MnO (110) MR				
PBE	−9.3	−2.6	4.5	2.1	5.1	−2.5	−0.8
PBE+U	−7.2	−3.5	2.7	0.3	4.0	−0.1	−0.5

ations, and advise to interpret with care the data obtained for other transition metal oxides such as NiO, MgO, and CaO. Further very recent experiments[9,10] do not straighten the understanding of the structural picture, which remains rather puzzling. In fact, although both sets of data indicate the formation of a small surface buckling, the physical interpretation is conflicting, since LEED and MEIS assign the observed outward relaxation to either surface O or Mn atoms, respectively. As a matter of fact, the LEED data listed in Table IV are affected by very large errors which render almost impossible any clear interpretation. Similarly to experiment, available LDA based *ab initio* calculations[11] and semiclassical MD simulations[10] depict an opposing description of the surface buckling b_1. Within this discouraging picture, our results might shed some light on this point and contribute to a more accurate understanding of the surface geometry of MnO(100). Although quantitatively different, as expected, the PBE and PBE+U results describe the same physics: The obtained values support the MD and LEED observations by assigning the surface buckling to a significant displacement of O atoms towards the vacuum side relative to the respective Mn atoms, which relax inwards. The surface rumpling b_1 is compensated by an opposite buckling in the subsurface layer (b_2). In the third layer the buckling almost disappears and the bulklike geometry is reestablished, in agreement with the LDA results. Overall, PBE+U provides smaller interlayer relaxations (d_{ij}) than PBE, in line with MEIS data. Generally, the observed relaxations are very small.

Due to the lack of experimental information on the structural properties of the (110) termination, our optimized geometry aims to be predictive, in particular the PBE+U structure of the (110) MR surface which was found to be more stable. Similar to the (100) termination, a positive surface buckling (i.e., outward displacement of topmost O atoms), which decreases significantly in deeper layers, is observed. As for the interlayer distances the situation is different. The two topmost layers experience considerable contractions, partially compensated by a substantial positive reduction of d_{34}, whereas $d_{45} \approx 0$. Therefore in the center of the slab the bulklike geometry is reproduced. Compared to the unreconstructed surface, the formation of the MR structure induces structural changes more localized in the first layer (the buckling in deeper layers disappears), reflecting the availability of more free space for the topmost species (due to the removal of 50% of surface atoms) which can be more easily accommodated at the surface.

C. Electronic structure

We focus now on the electronic properties of the MnO terminations in terms of the PBE+U layer-projected density of states (DOS) displayed in Figs. 4–6. To stress the better description provided by PBE+U we also show the DOS calculated within PBE, where the insulating nature of MnO is significantly underestimated. Since the changes induced by the surface are well-localized on the outermost layers and disappear quickly deeper down in the slab, the DOS is plotted only for the surface, subsurface, and the central layer. In the latter, the bulklike features are resembled for all three

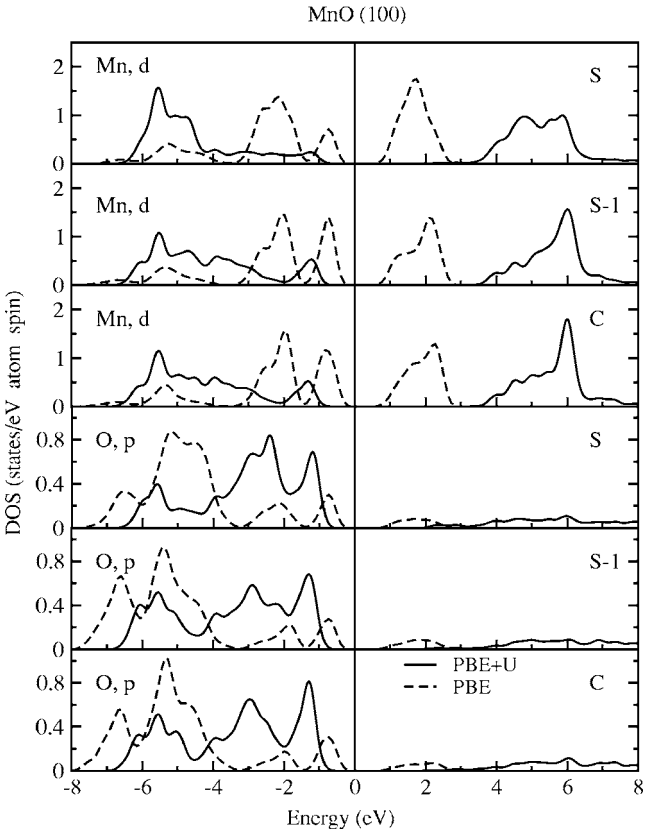

FIG. 4. PBE+U and PBE layer and spin resolved density of states for (a) MnO(100). S, S-1, and C refer to surface, subsurface, and center layer, respectively.

terminations. Similarly to NiO(100)[26] a decrease of the insulating gap near the surface is observed, though for MnO this effect is significantly reduced within PBE+U: The reduction of the gap is not dramatic (see Fig. 4), it decreases by about 0.15 eV with respect to the bulk value (2.03 eV)—in agreement with previous calculations[11]—whereas for the (110) surface the substantial weakening of the insulating nature plays a crucial role in driving the MR structural transition. From Fig. 5 it appears clear that an upward shift of the occupied O p states associated with a downward movement of the unoccupied Mn d states accompanied by an even larger displacement of the unoccupied O p orbitals towards the Fermi energy destroys the intermediate Mott-Hubbard/charge-transfer insulating character of MnO. The highest occupied states lose their mixed Mn d-O p character, which reduces the insulating nature of this surface considerably (band gap $\approx$0.5 eV). All that affects remarkably the stability of the bulk terminated (110) surface. By undergoing the MR reconstruction, the (110) surface experiences only a small reduction of the band gap [1.66 eV, see Fig. 6, comparable to that observed for MnO(100)], and gains stability in terms of surface energy, as discussed before. We can conclude that the physics behind the formation of the MR reconstruction is the stabilization of the insulating character of MnO, which would be otherwise lost. Furthermore, the MR structural transition is accompanied by a strong stabilization of the AFM II magnetic ordering, as discussed in the next section.

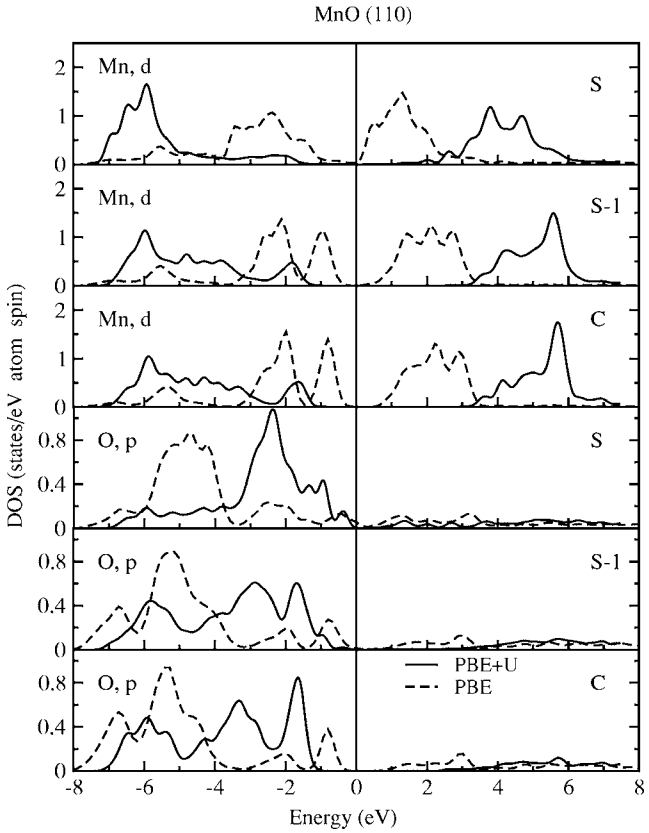

FIG. 5. PBE+U and PBE layer and spin resolved density of states for MnO(110). S, S-1, and C refer to surface, subsurface, and center layer, respectively.

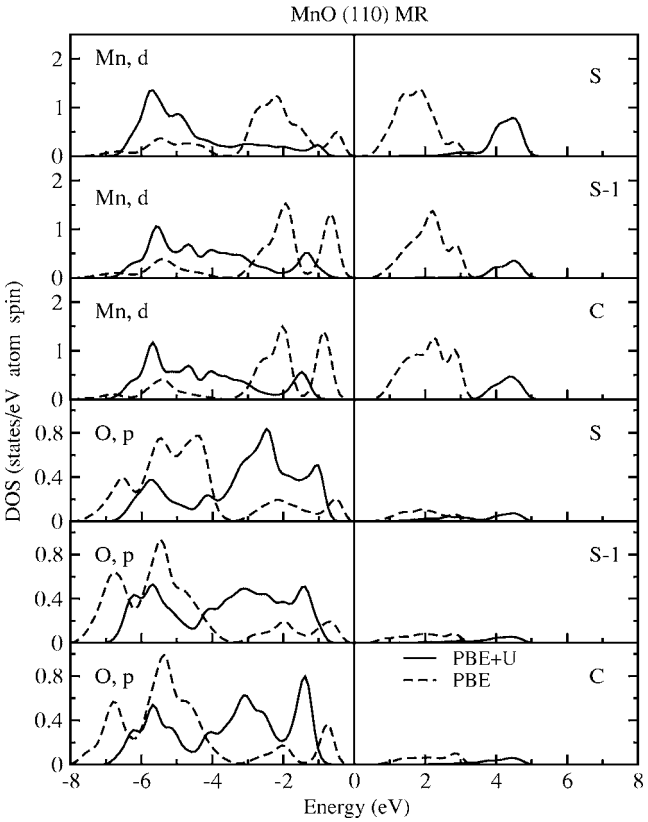

FIG. 6. PBE+U and PBE layer and spin resolved density of states for MnO(110) MR. S, S-1, and C refer to surface, subsurface, and center layer, respectively.

D. Magnetic interactions

For all surface orientations almost identical layer resolved Mn magnetic moments are found, practically equal to those evaluated in the bulk (PBE+U:4.69μ_B). At the surface very small moments are induced on the O atoms ($\approx$0.03μ_B). This is in analogy to observations for other metal oxide surfaces, such as NiO(100)[39] and CoO(100).[40] Interestingly, this picture differs substantially from what is found at the bulk terminated (111) polar surface, where a rather large reduction of the surface Mn magnetic moments ($\mu_{Mn} \approx 4.3\mu_B$) and a significant induction of magnetic moment into the outermost O atoms ($\approx$0.3μ_B) was observed.[4]

The magnetic properties of the MnO terminations have been analyzed by extracting the exchange coupling constants out of total energy differences within an adequate set of different magnetic configurations. For simplicity and to shorten the computational effort we have assumed the following simplifications: (i) unlike the calculations of the AFM II ground state we restrict ourself to smaller slabs of 7, 9, and 11 layers for the (100), (110), and (110) MR surfaces, respectively; we believe that this approximation will not significantly affect our final results since the changes induced by the surface are generally limited to the uppermost layers [it has been shown for NiO(100)[26] that very similar results are obtained within a 7 or 11 layer slab]. In addition, to cut the number of magnetic configurations to be taken into account, (ii) we have calculated the surface parallel components for MnO(100) only.

In Table II an overview of the magnetic orderings considered and the corresponding relative stability is presented. Besides the FM and the AFM II arrangements nine other configurations were taken into consideration, whose schematic layer projected description is also displayed. In case of the MnO(100) the calculation of $J^S_{1\parallel}$ and $J^S_{2\parallel}$ requires a doubling [AFM 8, see Fig. 1(b)] or even a quadruplication [AFM 9, see Fig. 1(c)] of the 1×1 2D unit cell to allow for higher degrees of freedom for the in-plane spin alignment. The AFM II magnetic ordering is conserved for both terminations and found to be almost degenerate with the AFM type-I (here labeled AFM 6), which confirms the bulk picture. The relative stability of the AFM II ordering is particularly evident in the MR reconstructed surface, which suggests an increase of the Néel temperature at the surface.

The influence of cutting the crystal on the exchange constants is summarized in Table V, where the values of the calculated magnetic interactions are listed. The labeling adopted follows a simple rule: the apex index (S, S-1, …) indicates the reference layer for which the NN and NNN interactions are evaluated. In the (100) geometry J_1 connects NN spins lying in adjacent layers, whereas in the (110) structure each atom possesses four nearest neighbors placed on the adjacent layer *and* one more on the subsequent layer, as illustrated in Fig. 2(b). For both terminations J_2 interacts between two NNN Mn atoms who are interconnected via an O atom [see Figs. 1(a) and 2(b)]. The results show that for all terminations the surface NN perpendicular component $J^S_{1\perp}$ is

TABLE V. Exchange integrals for MnO(100) (unreconstructed and fully relaxed slabs), MnO(100), MnO(110), and MnO(110) MR surfaces (in meV). The bulk values are J_1=0.71 meV and J_2 =0.36 meV, taken from Ref. 3.

	(100)-unr	(100)	(110)	(110) MR
$J^S_{1\perp}$	0.80	0.86	0.90	1.08
$J^{S-1}_{1\perp}$	0.78	0.70	0.62	0.67
$J^{S-2}_{1\perp}$	0.79	0.72	0.76	0.83
$J^{S-3}_{1\perp}$			0.70	0.72
$J^S_{2\perp}$	0.77	0.85	0.78	1.51
$J^{S-1}_{2\perp}$	0.56	0.57	0.22	0.73
$J^{S-2}_{2\perp}$			0.51	0.20
$J^{S-3}_{2\perp}$				0.48
$J^S_{1\parallel}$	0.44	0.53		
$J^S_{2\parallel}$	0.37	0.40		

enhanced by at least 25% compared to those in the bulk, whereas deeper perpendicular constants remain essentially unaffected (the value in the middle of the slab is identical to the one in the bulk). For the next nearest neighbor interactions an overall bigger increase is found, which, though stronger at the surface ($J_{2\perp}$ has twice the bulk value), is remarkably large in the innermost layers, especially for the (100) termination, where $J_{2\perp}$ experiences a double increase as compared to $J_{1\perp}$. The only exceptions are $J^{S-1}_{2\perp}$ and $J^{S-2}_{2\perp}$ for the (110) and (110) MR terminations, respectively, which are reduced by almost 40%. However, by taking the average value of $J_{2\perp}$ in the two deeper layers one obtains exactly the bulk value of J_2. The main difference induced by the MR reconstruction on the magnetic interactions in the (110) termination concerns the NNN coupling at the surface, namely $J^S_{2\perp}$: for the reconstructed surface its value is almost twice as large, thus reflecting the enhanced stability of the AFM II arrangement with respect to all other magnetic orderings.

Via the AFM 8 and AFM 9 magnetic configuration the in-plane exchange coupling constants for MnO(100) were evaluated to be $J^S_{1\parallel}$=0.53 meV and $J^S_{2\parallel}$=0.40 meV.

In order to see the effect of surface relaxations on the exchange parameters, we have also computed their values for the ideal bulk terminated unreconstructed MnO(100) surface. The corresponding values are listed in the first column of Table V. As expected, the variations are very small, in line with the small relaxations observed for the (100) termination reported in Table IV. However, we see that unlike the fully relaxed surface, in the unrelaxed slab the magnitudes of $J^{S-1}_{1\perp}$ and $J^{S-2}_{1\perp}$ are found to be ≈10% larger than the bulk value of J_1, thus reflecting the weak instability of such ideal termination.

We should stress at this point that the total energy differences entering the formalism are very small, providing small values for the exchange coupling constants, which is consistent with the experimental picture (as a touchstone, one should consider that the exchange interactions in NiO are two orders of magnitude larger than in MnO, due to the much higher Néel temperature, T_N=524 K). The small energy differences involved (10^{-4} eV) make therefore a precise quantitative estimation of the J's quite difficult.

In conclusion, an overall enhancement of the perpendicular surface exchange coupling constants was found for all surfaces which validates the arguments of Pothuizen *et al.*[41] and confirms the picture described by Ködderitzsch *et al.*[26] on the NiO(100) surface. In that case the authors find that the exchange coupling experiences a pronounced increase along the direction perpendicular to the surface (≈25%) and a slight reduction within the outermost layer. These findings on the MnO and NiO surfaces weaken the impact of earlier embedded cluster calculations on the transition metal monoxide surfaces MnO, FeO, CoO, NiO, and CuO (Ref. 42) reporting a general reduction of the exchange coupling at the surface.

IV. CONCLUSIONS

In conclusion, we have presented a study of the structural, electronic, and magnetic properties of MnO(100) and (110) surfaces. We have shown that the PBE+U approach improves over a standard PBE description and is able to describe the fundamental ground state properties of the MnO surfaces. Our results suggest that most of the modifications induced by the truncation of the crystal are localized near the surfaces. The experimental controversial surface rumpling of the (100) surface stems from an outward relaxation of the topmost O. Interestingly, the MnO(110) shows a spontaneous tendency to reconstruct into a MR type structure, the origin of that being the stabilization of the insulating regime at the surface which would be strongly reduced at the bulk terminated surface. As a consequence, we predict a strongly enhanced stabilization of the AFM type-II ordering. Despite the substantial gain in surface energy induced by the MR transition (≈30 meV/Å^2), the (100) surface remains favored over the (110) MR by about 24 meV/Å^2. The electronic changes indicate a slight reduction of the bulk insulating gap, provoked by a shift of the valence band which retains a mixed Mn d-O p character. Finally, though the Mn magnetic moment remains unchanged with respect to the bulk, the calculation of the exchange coupling constants points out an extensive pronounced increase of the perpendicular interactions and a small weakening of the parallel in-plane component. The global changes on the magnetic structure would suggest an increase of the surface Néel temperature, especially for the MR structure, to be confirmed by experiment.

ACKNOWLEDGMENTS

Financial support by the Austrian Science Fund FWF within the Joint Research Program S90 and the Science College W4 is gratefully acknowledged.

APPENDIX

In this Appendix, we list the set of equations used to compute the magnetic coupling parameters for the MnO(100), MnO(110), and MnO(110) MR terminations. We have calculated the exchange parameters via energy differences of the different magnetic phases summarized in Table

II, within an Ising type approach. The labeling is straightforward: H^{FM} corresponds to the DFT total energy of the FM ordering, whereas $H^1, H^2, \ldots, H^9$ represent the DFT total energies for the AFM 1, AFM 2,…, AFM 9 configurations.

1. MnO(100)

$$J_1^S = \frac{1}{48S^2}(H^{FM} + H^4 - H^8 - H^9) - \frac{2}{3}J_2^S,$$

$$J_2^S = -\frac{1}{64S^2}(2H^8 - H^{FM} - H^4),$$

$$J_{1\perp}^S = \frac{1}{128S^2}[H^1 + H^2 - H^6 - H^7],$$

$$J_{1\perp}^{S-1} = \frac{1}{128S^2}[H^{FM} - H^2 + H^7 - H^3],$$

$$J_{1\perp}^{S-2} = \frac{1}{128S^2}[H^{FM} - H^1 + H^3 - H^6],$$

$$J_{2\perp}^S = \frac{1}{32S^2}[H^1 - H^5 + H^3 - H^7],$$

$$J_{2\perp}^{S-1} = \frac{1}{32S^2}[H^{FM} - H^1 + H^6 - H^3].$$

2. Unreconstructed MnO(110)

$$J_{1\perp}^S = \frac{1}{32S^2}(H^{FM} - H^2 + H^4 - H^5),$$

$$J_{1\perp}^{S-1} = J_{1\perp}^S - \frac{1}{32S^2}[H^6 + H^4 - H^5 + H^{FM} - H^3 - 2H^2 + H^7],$$

$$J_{1\perp}^{S-2} = \frac{1}{32S^2}(H^1 - H^3 - H^4 - H^7),$$

$$J_{1\perp}^{S-3} = \frac{1}{32S^2}[H^{FM} - H^1 - H^5 - H^6],$$

$$J_{2\perp}^{S,S-2} = \frac{3}{2}J_{1\perp}^S - \frac{1}{8S^2}(H^4 - H^5),$$

$$J_{2\perp}^{S-1,S-3} = 2J_{1\perp}^S - \frac{5}{2}J_{1\perp}^{S-1} + \frac{1}{8S^2}(H^2 - H^7),$$

$$J_{2\perp}^{S-2,S-4} = \frac{1}{8S^2}(H^{FM} - H^1) - \frac{1}{2}J_{1\perp}^{S-2} - 2J_{1\perp}^{S-3}.$$

3. MnO(110) MR

$$J_{1\perp}^S = \frac{1}{28S^2}[H^{FM} - H^4 - H^6 + H^7],$$

$$J_{1\perp}^{S-1} = \frac{1}{64S^2}[H^{FM} - H^5 - H^2 + H^9] - \frac{1}{8}J_{1\perp}^S - \frac{1}{4}J_{2\perp}^S,$$

$$J_{1\perp}^{S-2} = \frac{1}{64S^2}[H^4 - H^2 - H^8 + H^3] + \frac{28}{64}J_{1\perp}^S - J_{1\perp}^{S-1},$$

$$J_{1\perp}^{S-3} = \frac{1}{64S^2}[H^2 - H^8 + H^4 - H^3 - 2H^{FM} + 2H^1] + J_{1\perp}^{S-4} - \frac{1}{16}J_{1\perp}^S,$$

$$J_{1\perp}^{S-4} = \frac{1}{64S^2}[H^{FM} - H^1 + H^8 - H^7],$$

$$J_{2\perp}^S = \frac{1}{16S^2}[H^{FM} - H^4 + H^6 - H^7],$$

$$J_{2\perp}^{S-1} = \frac{1}{32S^2}[H^{FM} - H^5 + H^2 - H^9] - \frac{1}{2}J_{1\perp}^{S-1},$$

$$J_{2\perp}^{S-2} = \frac{1}{32S^2}[H^4 - H^3 - H^2 + H^8] - \frac{1}{2}J_{1\perp}^{S-2} - \frac{1}{8}J_{1\perp}^S,$$

$$J_{2\perp}^{S-3} = \frac{(H^{FM} - H^1)}{16S^2} - \frac{1}{2}J_{1\perp}^{S-3} - 2J_{1\perp}^{S-4}.$$

*Electronic address: veronika.bayer@univie.ac.at
†Also at INFM-SLACS, Sardinian Laboratory for Computational Materials Science, University of Cagliari, Italy.

[1] I. P. R. Moreira, F. Illas, and R. L. Martin, Phys. Rev. B **65**, 155102 (2002).
[2] J. Muscat, A. Wander, and N. M. Harrison, Chem. Phys. Lett. **342**, 397 (2001).
[3] C. Franchini, V. Bayer, R. Podloucky, J. Paier, and G. Kresse, Phys. Rev. B **72**, 045132 (2005).
[4] C. Franchini, V. Bayer, R. Podloucky, G. Parteder, S. Surnev, and F. P. Netzer, Phys. Rev. B **73**, 155402 (2006).
[5] R. C. Felton, M. Prutton, S. P. Tear, and M. R. Welton-Cook, Surf. Sci. **88**, 474 (1979).
[6] M. A. Langell and N. R. Cameron, Surf. Sci. **185**, 105 (1987).
[7] M. A. Langell, C. W. Hutchings, G. A. Carson, and M. H. Nassir, J. Vac. Sci. Technol. A **14**, 1656 (1996).
[8] F. Müller, R. de Masi, D. Reinicke, P. Steiner, S. Hüfner, and K. Stöwe, Surf. Sci. **520**, 158 (2002).

[9] E. A. Soares, R. Paniago, V. E. de Carvalho, E. L. Lopes, G. J. P. Abreu, and H. D. Pfannes, Phys. Rev. B **73**, 035419 (2005).
[10] T. Okazawa and Y. Kido, Surf. Sci. **556**, 101 (2004).
[11] H. Momida and T. Oguchi, J. Phys. Soc. Jpn. **72**, 588 (2003).
[12] C. de Graaf, R. Boer, and W. C. Nieuwport, Chem. Phys. Lett. **271**, 372 (1997).
[13] D. C. Chrzan and L. M. Falicov, Phys. Rev. Lett. **61**, 1509 (1988).
[14] G. Kresse and J. Hafner, Phys. Rev. B **48**, 13115 (1993).
[15] G. Kresse and J. Furthmüller, Comput. Mater. Sci. **6**, 15 (1996).
[16] P. E. Blöchl, Phys. Rev. B **50**, 17953 (1994).
[17] G. Kresse and D. Joubert, Phys. Rev. B **59**, 1758 (1999).
[18] J. P. Perdew, K. Burke, and M. Ernzerhof, Phys. Rev. Lett. **77**, 3865 (1996).
[19] V. I. Anisimov, J. Zaanen, and O. K. Andersen, Phys. Rev. B **44**, 943 (1991).
[20] S. L. Dudarev, G. A. Botton, S. Y. Savrasov, C. J. Humphreys, and A. P. Sutton, Phys. Rev. B **57**, 1505 (1998).
[21] M. Methfessel and A. T. Paxton, Phys. Rev. B **40**, 3616 (1989).
[22] H. J. Monkhorst and J. D. Pack, Phys. Rev. B **13**, 5188 (1976).
[23] B. E. F. Fender, A. J. Jacobson, and F. A. Wegwood, J. Chem. Phys. **48**, 990 (1968).
[24] R. W. G. Wyckoff, *Crystal Structures* (Interscience, New York, 1964).
[25] R. L. Martin and F. Illas, Phys. Rev. Lett. **79**, 1539 (1997).
[26] D. Ködderitzsch, W. Hergert, W. M. Temmerman, Z. Szotek, A. Ernst, and H. Winter, Phys. Rev. B **66**, 064434 (2002).
[27] I. de P. R. Moreira and F. Illas, Phys. Chem. Chem. Phys. **8**, 1645 (2006).
[28] M. E. Lines, Phys. Rev. **139**, A1304 (1965).
[29] M. E. Lines and E. D. Jones, Phys. Rev. **139**, A1313 (1965).
[30] T. Oguchi, K. Terakura, and A. R. Williams, Phys. Rev. B **28**, 6443 (1983).
[31] P. M. Oliver, G. W. Watson, and S. C. Parker, Phys. Rev. B **52**, 5323 (1995).
[32] B. Warot, E. Snoeck, P. Baulès, J. C. Ousset, M. J. Casanove, S. Duborg, and J. F. Bobo, J. Cryst. Growth **224**, 309 (2001).
[33] B. Warot, E. Snoeck, J. C. Ousset, M. J. Casanove, S. Duborg, and J. F. Bobo, Appl. Surf. Sci. **188**, 151 (2002).
[34] O. Begone, M. Alouani, J. Hugel, and P. Blöchl, Comput. Mater. Sci. **24**, 192 (2002).
[35] T. Okazawa, Y. Yagi, and Y. Kido, Phys. Rev. B **67**, 195406 (2003).
[36] A. Rohrbach, J. Hafner, and G. Kresse, Phys. Rev. B **69**, 075413 (2004).
[37] C. Sousa, C. de Graaf, N. Lopez, N. M. Harrison, and F. Illas, J. Phys.: Condens. Matter **16**, S2557 (2004).
[38] M. Prutton, J. A. Walker, M. R. Welton-Cook, and R. C. Felton, Surf. Sci. **89**, 95 (1979).
[39] S. L. Dudarev, A. I. Liechtenstein, M. R. Castell, G. A. D. Briggs, and A. P. Sutton, Phys. Rev. B **56**, 4900 (1997).
[40] M. R. Castell, S. L. Dudarev, G. A. D. Briggs, and A. P. Sutton, Phys. Rev. B **59**, 7342 (1999).
[41] J. Pothuizen, O. Chen, and G. Sawatzky, Mater. Res. Soc. Symp. Proc. **401**, 501 (1996).
[42] V. Staemmler and K. Fink, Chem. Phys. **278**, 79 (2001).